Journal of Membrane Science 662 (2022) 121004

Contents lists available at ScienceDirect

Journal of Membrane Science

journal homepage: www.elsevier.com/locate/memsci

Thermotolerant separator of cross-linked polyimide fibers with narrowed pore size for lithium-ion batteries

Yang Wang, Minhao Guo, Hui Fu, Zhenzhong Wu, Yizhe Zhang, Guojie Chao, Suli Chen, Longsheng Zhang *, Tianxi Liu **

Key Laboratory of Synthetic and Biological Colloids, Ministry of Education, School of Chemical and Material Engineering, Jiangnan University, Wuxi, 214122, China

ARTICLE INFO

Keywords:
Lithium-ion battery
Separator
Thermal stability
Electrospun membrane
Polyimide

ABSTRACT

Separators are of significance in the thermal safety and energy-storage performance of lithium-ion batteries (LIBs). Thermotolerant separators of electrospun polyimide (PI) fibers hold great promise as candidate to commercial polyolefin-based separators due to their high thermal and electrochemical stability. However, their applications in LIBs are limited by the undesirably large pore size (~2 μm) that will induce dendrite growth and thermal runaway of batteries. Here, we demonstrate a facile and scalable strategy to prepare thermotolerant separators of cross-linked PI fibers (c-PI) with a narrowed pore size (0.78 μm) via a blended electrospinning of polyamic acid and polystyrene followed by a thermal imidization. The electrospun fibers in the c-PI separator are ribborn-like and feature adhesion structure between adjacent fibers, while no such structures are observed for PI separator obtained without adding polystyrene. In comparison with the PI separators, the c-PI separator exhibits higher porosity, better electrolyte adsorption and higher ionic conductivity. In Comparison to the batteries with PI and Celgard separators, the battery with c-PI separator shows greatly enhanced electrochemical performance with a high capacity of 100.1 mAh/g at 10 C after 1600 cycles. This work offers a feasible and effective route to develop advanced membranes of electrospun fibers for safe LIBs.

1. Introduction

Lithium-ion batteries (LIBs) have been widely used as energy-storage devices in applications of portable electronics and electric vehicles, owing to their high energy densities and long cycling life [1–4]. The LIB is generally consisted of cathode, anode, electrolyte and separator [5,6]. Notably, the separator plays a vital role in the battery, it can not only prevent internal short circuit *via* separating and avoiding electronic contact between the cathode and anode [7], but also retain liquid electrolyte and allow free transportation of lithium ions [8,9]. Currently, the most commercialized separators are the polyolefin-based membranes because of their good electrochemical stability and mechanical property [10], which unfortunately show some inherent drawbacks including poor electrolyte wettability, low porosity and thermal stability [11–13]. For instance, owing to their internal low melting temperature, the commercial separators of polyethylene (PE) or polypropylene (PP) would shrinkage at high temperature (>140 °C), which would induce an internal short circuit and eventually result in safety problems with fire or even explosion [14,15].

In this regard, great efforts based on advanced nanotechnology have been devoted to overcome the aforementioned drawbacks of polyolefin-based separators [16–19]. One of the widely-used strategies is coating the polyolefin-based separators with ceramic materials (SiO_2, TiO_2, Al_2O_3, ZrO_2, etc.) to promote their thermal performance and electrolyte affinity [20–23]. Unfortunately, the coated ceramic materials would easily detach from the separators due to the poor attachment, resulting in pore blockage of separator and performance deterioration of battery [24,25]. Alternatively, a feasible strategy to develop thermotolerant separators is replacing polyolefin by other material with high thermal stability [26]. Notably, polyimide (PI) is considered as a prospective candidate because of its high thermal stability of ~450 °C, as well as its good mechanical property and electrochemical stability [27]. However, polyimide with aromatic groups is usually infusible and insoluble, which increase the requirement of manufacture and limit its applicability [28]. To date, compared with the other two main methods to prepare PI separators (template and phase-inversion method) [29–33], the

* Corresponding author.
** Corresponding author.
E-mail addresses: zhangls@jiangnan.edu.cn (L. Zhang), txliu@jiangnan.edu.cn (T. Liu).

https://doi.org/10.1016/j.memsci.2022.121004
Received 26 July 2022; Received in revised form 2 September 2022; Accepted 14 September 2022
Available online 22 September 2022

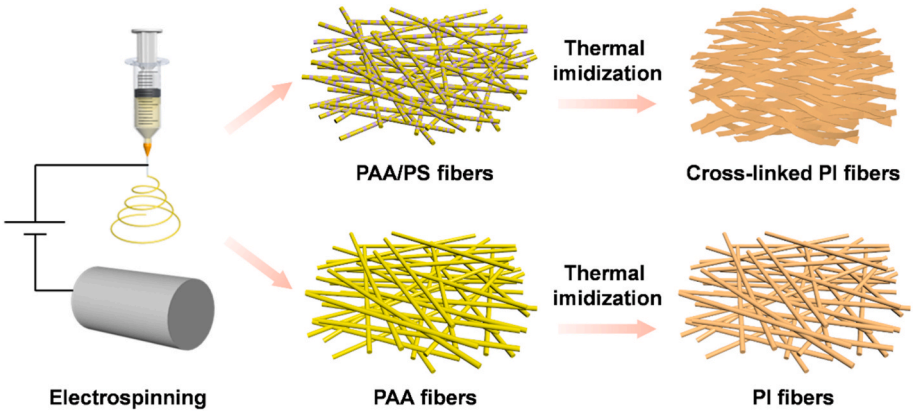

Fig. 1. Schematic of the preparation process of cross-linked PI and PI separators.

electrospinning method is more facile and scalable, where the resulting membranes with PI-fiber networks possess many advantageous features including high porosity and large specific surface area [34,35]. Miao et al. reported the design and fabrication of PI fiber-based membranes through electrospinning method and their applications as separators in LIBs, which showed higher thermal stability, stronger affinity with electrolytes and higher ionic conductivity compared to polyolefin-based separators [36].

Unfortunately, the electrospun PI fiber-based membranes usually present large pore size (~2 μm) with an uneven pore-size distribution [37]. A large pore size would prone to cause self-discharge phenomena, and an uneven pore-size distribution would lead to an uneven flux of lithium ions that can induce micro-short circuit derived from undesired growth of lithium dendrites [38–40]. Li et al. applied the phase-field simulations to study the influence of pore size on inhibiting lithium dendrites, and they found that the maximum height of lithium dendrites would drastically increases when the pore size increases above 1 μm [41]. According to the operation standards of Li-ion batteries released by the United States Advanced Battery Consortium, the separators with a uniform pore size of <1 μm are required for robust and durable operation [42]. Dendrite growth in Li-ion batteries could induce thermal runaway of battery at high current densities, which would remain a safety hazard with their large-scale application in portable electronic or electric vehicles [43,44]. Besides, under working conditions, a great amount of heat will be generated that would also give rise to a thermal runaway of battery, especially when the battery is subjected to mechanical or thermal abuse [45,46]. Thus, developing thermotolerant separator of electrospun PI fibers with narrow pore sizes and good dendrite inhibition is urgently desired.

Here, we report a feasible and scalable approach to prepare thermotolerant membranes of cross-linked PI fibers (c-PI) with adhesion structure between the adjacent fibers via electrospinning of a mixed precursor of polyamic acid (PAA) and polystyrene (PS), followed by thermal imidization. The resulting c-PI membrane has a narrowed pore-size of 0.78 μm, and it possesses a high thermal stability with no shrinkage at 250 °C. Benefiting from the electrospinning method, the c-PI membrane has an inherently high porosity of 81%, much higher than the commercial Celgard separators. Furthermore, in comparison to the Celgard separators, the c-PI separator exhibits higher electrolyte uptake (540.2%), stronger affinity for electrolytes with a contact angle of almost 0°, and higher ionic conductivity of 1.1 mS/cm. The electrochemical measurements reveal that the $LiFePO_4$|Li battery with c-PI separator showed enhanced rate performance compared with that of Celgard separator. Besides, the battery with c-PI separator shows good cycling stability and retains a capacity of 100.1 mAh/g at 10 C after 1600 cycles, making it as a good separator candidate for applications in LIBs.

2. Experimental

2.1. Chemicals

4,4′-oxydianiline (ODA), pyromellitic dianhydride (PMDA), dimethylacetamide (DMAc), polystyrene (PS) and n-butanol were brought from Sinopharm Chemical Reagent Co., Ltd. Carbon black, polyvinylidene difluoride (PVDF) and lithium iron phosphate ($LiFePO_4$) were brought from Aladdin Technology Co., Ltd. Celgard 2500 separators were purchased and used as control samples. The liquid electrolyte used in this work is consisted of 1.0 M lithium hexafluorophosphate ($LiPF_6$) in mixture of ethlyene carbonate (EC) and diethyl carbonate (DEC) with volume ratio of 1/1.

2.2. Preparation of the PI and c-PI membranes

As illustrated in Fig. 1, the PI and c-PI membranes were obtained via a blended electrospinning of pure PAA and PAA/PS mixed solutions respectively, followed by thermal imidization. The PAA solution (15 wt %) was obtained by the polymerization of ODA and PMDA monomers (Fig. S1). Typically, 7.9 g ODA was first dissolved in 100 mL DMAc in a flask under N_2 flow for 15 min, followed by adding 8.6 g PMDA by five batches of an equivalent amount at 0 °C under continuous stirring for 12 h. The PS solution (15 wt%) was obtained by dissolving 16 g PS in 100 mL DMAc. The PAA/PS blended solutions (15 wt%) were prepared by mixing these two solutions at a weight ratio of 2/1. The electrospinning of PAA/PS mixed solutions were carried out using a spinning tower syringe of 0.5 mm in diameter. The resultant PAA/PS membranes were then subjected to a thermal imidization process, where the PAA/PS membranes were heated up at a rate of 5 °C/min to 100, 200, 300 and 350 °C, and held for 60 min at each temperature stage. The as-obtained membrane of cross-linked polyimide fibers is denoted as c-PI. Accordingly, pure PI membrane was synthesized *via* a similar procedure without adding PS. As shown in Fig. S2, the thickness of c-PI and PI membranes are both 24 μm, which are similar to that of commercial Celgard separator (25 μm).

2.3. Characterization and electrochemical measurement of separators

The porosity was calculated according to the following Eq. (1)

$$Porosity = \frac{Mw - Md}{\rho_b V_d} \times 100 \quad (1)$$

where M_w and M_d are the weights of the wet membrane (immersed in n-butanol for 2 h) and the dry membrane respectively, ρ_b is the density of n-butanol, and V_d is the apparent volume of the dry membranes.

The ionic conductivities of membranes were evaluated by using potentiostatic electrochemical impedance spectroscopy (EIS) between

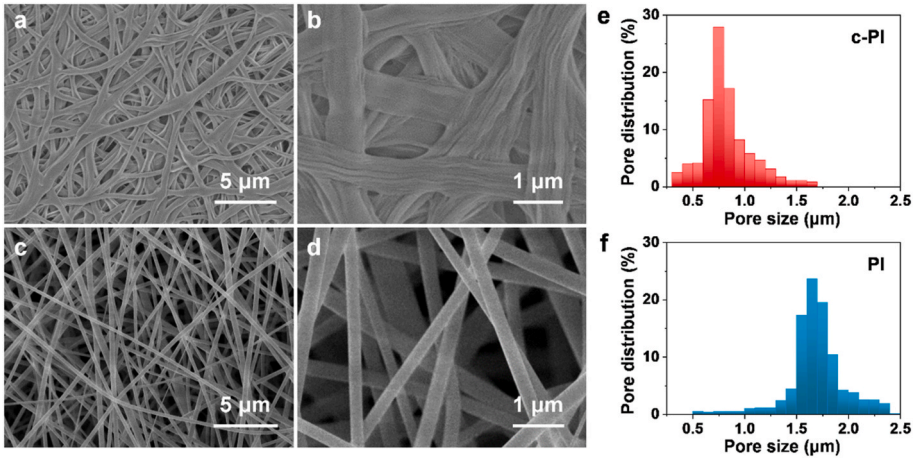

Fig. 2. SEM images of (a, b) c-PI and (c, d) PI samples. (e, f) Pore-size distribution of c-PI and PI, respectively.

1.0 MHz and 0.1 Hz. The EIS experiments were measured at 25 ± 2 °C under symmetric configuration in CR2032 coin cells, using stainless steel as blocking electrodes.

The ionic conductivities (σ) were calculated with Eq. (2)

$$\sigma = \frac{d}{R_b S} \tag{2}$$

where d is the thickness of the membrane, R_b is the bulk resistance, and S is the geometric area of the electrode, respectively.

The interfacial resistance of lithium metal and electrolyte was measured in a similar cell with two lithium metal electrodes. The potential window of separators was investigated by linear sweep voltammetry (LSV) measurement. The separators were placed between a stainless steel and a lithium metal electrode. LSV was conducted from open circuit voltage to 6.0 V vs. Li/Li^+ at 5 mV/s. Coin-type $Li|LiFePO_4$ cells were prepared to assess the battery performance of c-PI and PI separators. Li metal and $LiFePO_4$ electrode ($LiFePO_4$: carbon black: PVDF = 8:1:1 by weight) were used as anode and cathode, respectively. The cycling performance of cell was investigated at 10 C at 25 ± 2 °C.

3. Results and discussion

Scanning electron microscopy (SEM) observations of the c-PI and PI membranes (Fig. 2a–d) show that the electrospun fibers are randomly interconnected and constructed a three-dimensional network with porous structures. Notably, the c-PI membrane features a morphology of ribbon fibers with many groove-like nanostructures (Fig. 2a and b), while the fibers in the PI membrane are cylindrical (Fig. 2c and d). The pores of the c-PI membrane are smaller and more uniform than those of the PI membrane, which would be advantageous for even current distribution that can prevent lithium dendrite and avoid internal microshort circuit of battery. The difference between the morphologies of these membranes may be attributed to the cross-linking effect originated from the different thermal properties of the two polymers (PI and PS). During the thermal imidization process, the PAA phase would be converted into PI while the PS phase would melt and decompose (Fig. S3).

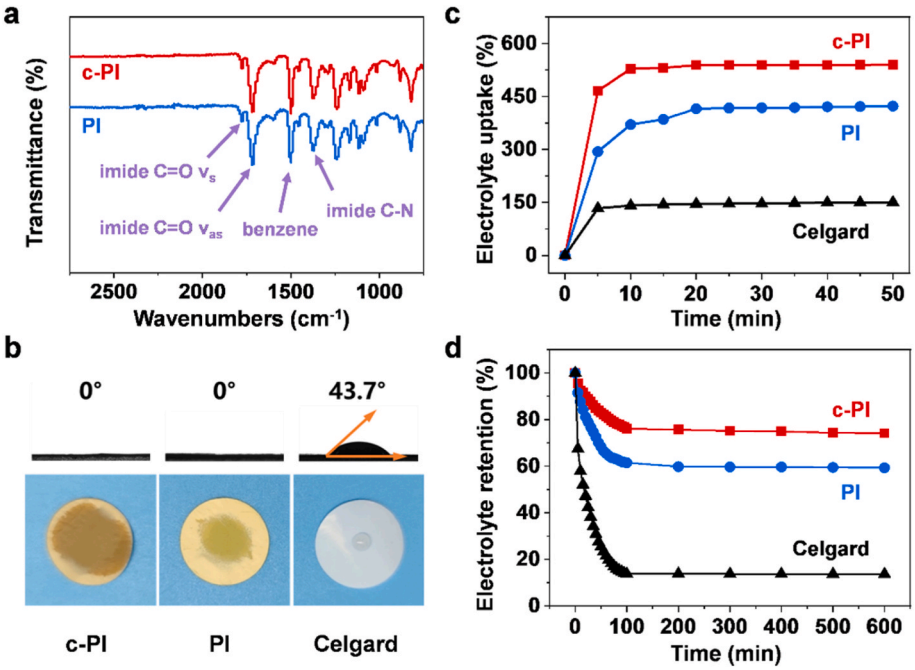

Fig. 3. (a) FTIR spectra of c-PI and PI. (b) Electrolyte contact angles of c-PI, PI and Celgard. (c, d) Electrolyte uptake and electrolyte retention of c-PI, PI and Celgard, respectively.

Table 1
Property parameters of the c-PI, PI and Celgard seperators.

Sample	Porosity (%)	Electrolyte uptake (%)	Electrolyte retention (%)	Contact angle (°)	Ionic conductivity (mS/cm)	Interfacial resistance (Ω)
c-PI	81	540.2	74.1	0	1.1	225.5
PI	73	422.7	59.2	0	0.6	250.2
Celgard	55	141.3	12.3	43.7	0.3	361.6

Because of the intermiscibility between PAA and PS, the melting PS would dissolve some PAA and lead to an adhesion structure between adjacent fibers that would finally convert to cross-linked PI fibers after the thermal imidization. Notably, the PAA/PS membrane before the thermal imidization features a morphology of cylindrical fibers (Fig. S4), which would finally convert to ribbon-like fibers with adhesion structures between adjacent fibers after the thermal imidization. The adhesion structures of fibers become prominent as the amount of PS component increases in the PAA/PS mixed solution for the blended electrospinning (Fig. S5). In comparison, the pure PAA membrane features a morphology of cylindrical fibers before and after the thermal treatment (Fig. S6).

As shown in Fig. 2e and f, we further study the pore sizes and pore-size distributions of c-PI and PI membranes using a PMI porometer. As expected, the c-PI membrane presented a narrow pore-size distribution ranging from 0.1 to 1.7 μm with an average size is 0.78 μm, which is smaller than that for the PI membrane (from 0.5 to 2.4 μm, with an average size of 1.63 μm). As displayed in Fig. S7, the synthesized c-PI and PI membranes both exhibit good flexibility and structural integrity when subjected to bending, twisting, wrinkling or unfolding. Besides, when the amount of PS component in the PAA/PS mixed solution increases, the mechanical property of the as-obtained c-PI membrane enhances (Fig. S8). The c-PI membrane prepared with a PAA/PS weight ratio of 2/1 exhibits greatly enhanced mechanical strength (26.4 MPa) than that of the PI membrane (6.7 MPa) owing to its adhesion structure between the adjacent fibers and the increased diameter of these fibers. Comparatively, the mechanical property of c-PI separator outperforms other reported electrospun PI-based separators (Table S1), which would enhance the safety of battery by mechanically restraining the growth of lithium dendrites.

We further carried out Fourier-transform infrared (FTIR) measurements to qualitatively analyze the chemical structure of c-PI and PI samples (Fig. 3a). The peaks at 1775 and 1720 cm^{-1} can be indexed to the symmetric vibration and asymmetric vibration of C═O stretching in imide structure, respectively. The peaks at 1500 and 1374 cm^{-1} can be related to the bending vibration of benzene rings and the C–N stretching of imide structure, respectively [47]. Such polar groups will enhance their compatibility with the electrolyte. As shown in Fig. 3b–d, we further investigate the absorption and retention capacity of electrolytes for the c-PI and PI membranes, since such parameters are of significance for their performance in batteries. For a separator, good electrolyte wettability with high electrolyte uptake and retention would enable efficient and durable transportation of lithium ions during the long-term cycling process, leading in higher energy density and longer working life of battery [48]. Generally, the observed droplet size and contact angle can describe the affinity between the separator and electrolyte. As shown in Fig. 3b, the droplets of electrolyte quickly spread over the c-PI and PI separators, which can be attributed to their polar compatibility and three-dimensional connected network with pore structures. In sharp contrast, the droplet size of electrolyte on the Celgard separator was retained without obvious changes. The Celgard separator has an intrinsically poor compatibility with electrolyte because of its hydrophobic characteristic and low surface energy. As shown in Fig. 3b, the Celgard separator shows a poor wettability to the electrolytes with a contact angle of 43.7° while both the c-PI and PI separators exhibits contact angles of almost 0°, thus verifying the superior electrolyte

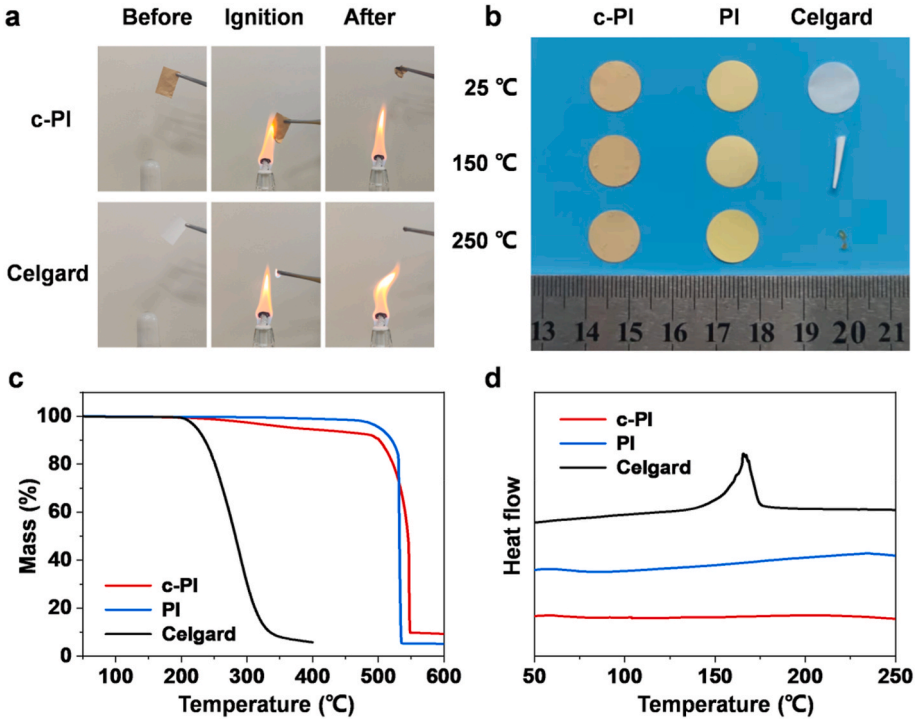

Fig. 4. (a) Digital images showing the flame-retardant properties of c-PI and Celgard. (b) Thermal shrinkage of c-PI, PI and Celgard kept at 25, 150 and 250 °C. (c, d) TG and DSC experiments of c-PI, PI and Celgard, respectively.

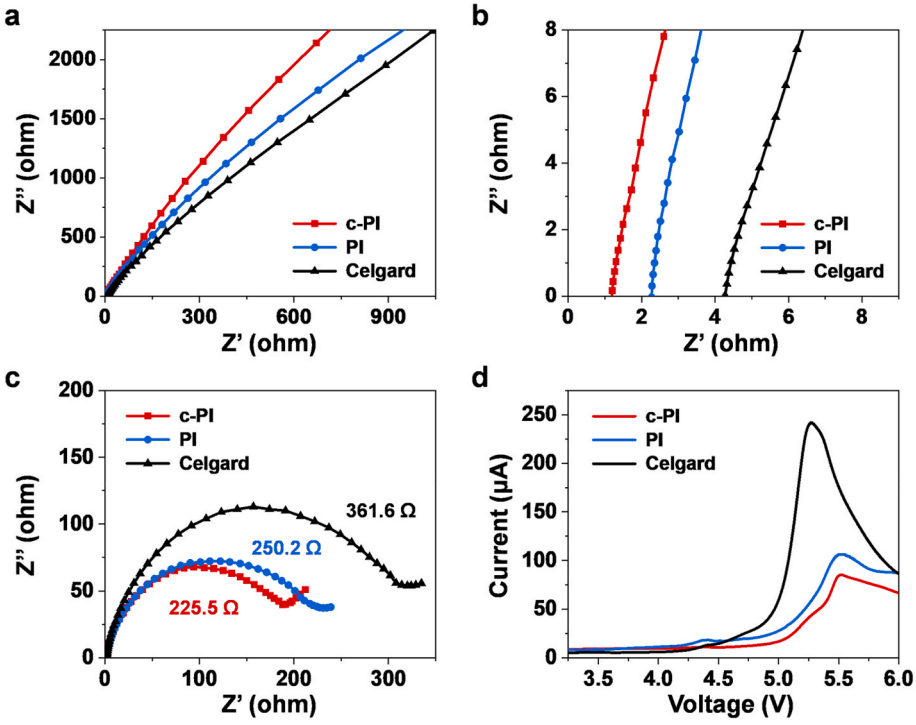

Fig. 5. (a, b) Nyquist plots of "stainless steel/separator/stainless steel" and (c) "Li/separator/Li" cells with the c-PI, PI and Celgard separators, respectively. (d) LSV curves of "Li/separator/stainless steel" cells with the c-PI, PI and Celgard separators.

wettability of c-PI and PI separators.

Electrolyte uptake and retention are also crucial factors for high-performance separators, which usually correlate with the porosity of separators. We further investigated the porosities of the c-PI and PI membranes using the n-butanol adsorption method, which is correlated with the specific surface area of membrane. The c-PI membrane shows a higher porosity of 81% in comparison with that (73%) of PI membrane, which may be attributed to the larger specific surface area of c-PI membrane (14.7 m^2/g) compared to that (6.9 m^2/g) of PI membrane (Fig. S9). Consequently, the electrolyte uptake of c-PI is higher than those of PI and Celgard (Fig. 3c and Table 1). Specifically, the electrolyte uptakes for c-PI, PI and Celgard reach 540.2%, 422.7% and 141.3% after 50 min, respectively. Furthermore, we investigated the electrolyte retention of these separators (Fig. 3d) and found that the electrolyte retention of c-PI, PI and Celgard stabilized at 74.1%, 59.2% and 12.3% after being held at 25 °C for 10 h, respectively. The improved electrolyte retention of c-PI separator may arise from its better affinity with electrolytes and smaller pore size.

As shown in Fig. 4, we further study the flame resistance and thermal stability of c-PI, PI and Celgard samples. The tests of flame-retardant performance (Fig. 4a and S10) reveal that the c-PI separator exhibits better flame-resistance and self-extinguishing property than Celgard separator that got burned violently after ignition. Comparatively, the c-PI separator with inherent thermotolerance show superior flame retardancy, which can deliver satisfactory safety of battery at elevated temperature. Fig. 4b shows the thermal-shrinkage behaviors of c-PI, PI and Celgard at 25, 150 and 250 °C for 60 min under air atmosphere, respectively. Notably, the c-PI and PI separators maintained their original shapes and showed no obvious shrinkage when heated at 250 °C. In comparison, the Celgard separator suffered from a large shrinkage at 150 °C and a total degradation when heated at 250 °C. The inferior thermal property of Celgard separator would cause physical contact between electrodes at elevated temperature [49]. We further carried out thermogravimetry (TG) and differential scanning calorimetry (DSC) experiments to explore the thermal properties of c-PI, PI and Celgard samples. The TG results (Fig. 4c) reveal that the c-PI and PI separators exhibit negligible weight loss at 450 °C while the Celgard separator has decomposed completely before that temperature. As shown in Fig. 4d, the Celgard separator shows an endothermic peak from 150 to 170 °C, representing to its softening and melting. Whereas, no obvious melting peaks below 250 °C are observed in the DSC thermograms for c-PI and PI separators.

We further carried out EIS with stainless steel as blocking electrode to investigate the ionic conductivity of separator (Fig. 5a and b). It can be seen that the bulk resistances of c-PI, PI and Celgard are 1.2, 2.2 and 4.3 Ω, respectively. The ionic conductivities for c-PI, PI and Celgard are 1.1, 0.6 and 0.3 mS/cm, respectively. The enhanced ionic conductivity of c-PI can be attributed to its larger liquid electrolyte uptake and retention that can promote the transport of lithium ions though the separator [50]. Besides, the Nyquist plots were conducted using "Li/Separator/Li" cells assembled with the c-PI, PI and Celgard separators. As shown in Fig. 5c, the interface resistance of the c-PI cell (225.5 Ω) is much smaller compared with those of the PI cell (250.2 Ω) and Celgard cell (361.6 Ω). These results, taken together, indicate that the c-PI separator can enable rapid ion transportation with smaller resistance, which may originate from its high structural porosity and large electrolyte uptake. With such features, the c-PI separator could reserve more quantity of electrolyte and promote the transfer of lithium ions through the channels. Further LSV experiments (Fig. 5d) are carried out to evaluate the electrochemical oxidation limits of separators. The PI and c-PI separators exhibit anodic stability at 5.0 V (vs. Li/Li^+), which is larger than that of Celgard separator (4.5 V), indicating their improved electrochemical stability. To evaluate the dendrite resistance of separators, we have assembled symmetrical Li||Li cells using c-PI and PI separators and carried out morphological observation for the surface of Li metal electrodes after 100 cycles of Li plating/stripping. The cycling tests were performed at a constant current density of 5 mAh/cm^2 at 25 ± 2 °C. As showed in Fig. S11, the Li metal obtained from the cell using PI separator features a rough surface with rod-like Li dendrites. Comparatively, the surface of Li metal from the cell with c-PI separator is more uniform and smoother with only a few small Li protrusions, indicating its better dendrite resistance than the PI separators.

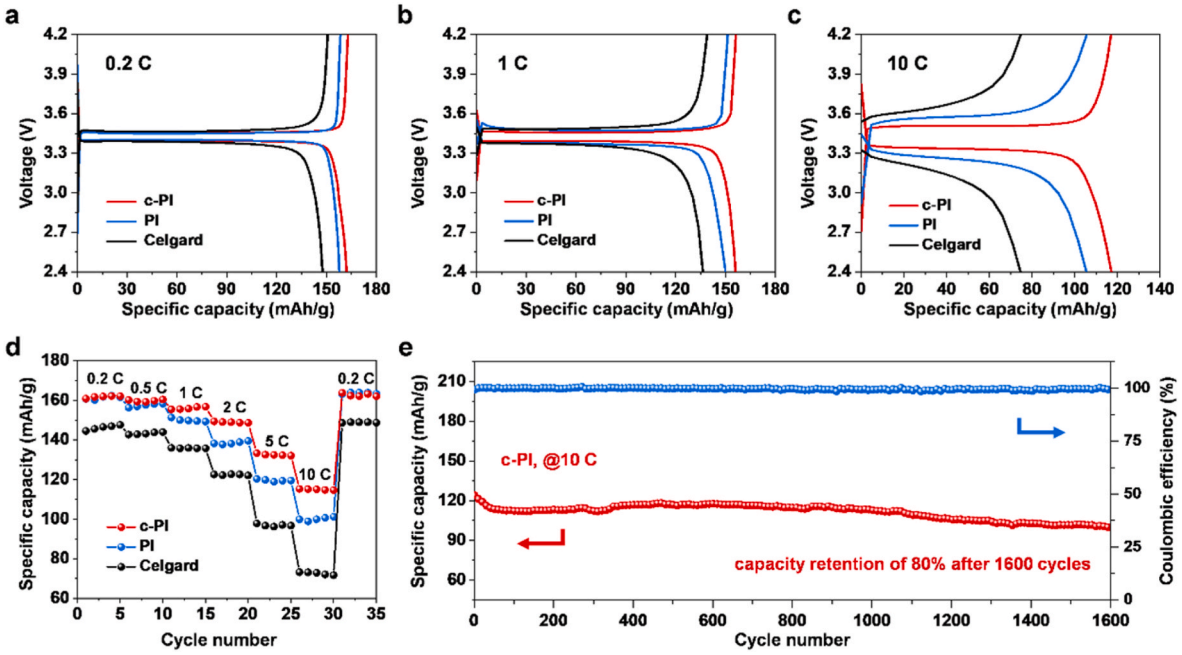

Fig. 6. (a–c) Charge/discharge curves of the 3rd cycle at 0.2, 1 and 10 C, respectively. (d) Specific capacities of the cells with c-PI, PI and Celgard separators at different current densities. (e) Cycling performance (left axis) and coulombic efficiency (right axis) of the cells with c-PI separator at 10 C.

Fig. 6a–c shows the charge-discharge curves of the 3rd cycle at 0.2, 1 and 10 C, respectively. The cells all showed stable discharge plateaus with specific capacities of 153, 161 and 166 mAh/g for Celgard, PI and c-PI separators at 0.2C, respectively. When the current density increased to 10 C, the capacities of the batteries with c-PI, PI and Celgard separators all decreased to some extent. The trend of decrement in specific capacity follows the orders of c-PI < PI < Celgard. The cell with c-PI separator shows a discharge capacity of 118 mAh/g at 10 C, higher than those of PI (105 mAh/g) and Celgard separator (74 mAh/g). Furthermore, the hysteresis of plateau potential in the charge/discharge profile is extremely high (0.13–0.64 V) and unstable for the cell with Celgard separator. In sharp contrast, the hysteresis of plateau potential in the charge/discharge profile for the cell with c-PI separator is lower (0.06–0.18 V) and more stable in spite of increasing the charge/discharge rates. As displayed in Fig. 6d, the discharge capacity of the cells with c-PI separator are higher at different current rates. And the ratios of capacity retention (10C/0.2C) for the cells with c-PI, PI and Celgard are 49%, 62% and 71%, respectively. As shown in Fig. S12, the charge transfer resistance of half-cells assembled with the c-PI separator is lower than those with PI and Celgard separators, which can promote the ion transfer process and improve the charge/discharge performance [51,52]. As shown in Fig. 6e and S13, the cycling measurement of the cell assembled with c-PI separator were carried out at 10 C. The initial discharge capacity of the cell with c-PI separator was 124 mAh/g and retained 113.2 mAh/g and 100.1 mAh/g after 1000 and 1600 cycles with retentions of 91% and 80%, respectively. During the stability test (Fig. 6e), it can be observed that the Coulombic efficiency is nearly 100%. Compared with other reported separators (Table S1), the cell with c-PI separator exhibits higher cycling stability, endowing the c-PI separator as a promising candidate for application in battery. Besides, the cell with c-PI separator exhibits a good cycling performance at elevated temperature (65 °C) and the Coulombic efficiency is above 95% (Fig. S14). Overall, the c-PI separator reported exhibited high electrolyte adsorption and good ionic conductivity, which can enable high rating capacity and cycling stability, thus endowing it as a prospective separator candidate for application in LIBs.

4. Conclusion

In summary, we report a scalable approach to prepare thermotolerant membrane of cross-linked PI fibers (c-PI) with narrowed pore size via blended electrospinning of PAA/PS followed by thermal imidization. The c-PI membrane features a morphology of interconnected networks of fibers with adhesion structure between adjacent fibers. The c-PI membrane presents a narrow pore-size distribution, and the average size is 0.78 μm, which is much smaller than that of PI membrane (1.63 μm) obtained without PS component. The c-PI separator exhibits higher porosity (81%), electrolyte uptake (540.2%) and ionic conductivity (1.1 mS/cm) than those of PI and Celgard separators. More importantly, the $LiFePO_4$|Li half-cells assembled with c-PI separator exhibit superior cycling stability and rating capacity compared with PI and Celgard separators, which can retain a high capacity of 100.1 mAh/g after 1600 cycles at 10 C.

CRediT authorship contribution statement

Yang Wang: Conceptualization, Investigation, Data curation, Writing - original draft. **Minhao Guo:** Investigation, Data curation. **Hui Fu:** Investigation, Data curation. **Zhenzhong Wu:** Data curation, Writing – review & editing. **Yizhe Zhang:** Data curation, Writing – review & editing. **Guojie Chao:** Writing – review & editing. **Suli Chen:** Writing – review & editing. **Longsheng Zhang:** Supervision, Resources, Writing – review & editing. **Tianxi Liu:** Supervision, Resources, Writing – review & editing.

Declaration of competing interest

The authors declare that they have no known competing financial interests or personal relationships that could have appeared to influence the work reported in this paper.

Data availability

Data will be made available on request.

Acknowledgements

This work was financially supported by the National Natural Science Foundation of China (52103260, 52161135302), Natural Science Foundation of Jiangsu Province (BK20210482) and Fundamental Research Funds for the Central Universities (2232019A3-03).

Appendix A. Supplementary data

Supplementary data to this article can be found online at https://doi.org/10.1016/j.memsci.2022.121004.

References

[1] C.F.J. Francis, I.L. Kyratzis, A.S. Best, Adv. Mater. 32 (2020), 1904205.
[2] Y.Q. Li, L. Yu, W.R. Hu, X.L. Hu, J. Mater. Chem. A 8 (2020) 20294–20317.
[3] Y. Xie, H.L. Zou, H.F. Xiang, R. Xia, D.D. Liang, P.C. Shi, S. Dai, H.H. Wang, J. Membr. Sci. 503 (2016) 25–30.
[4] Y. Hu, Y.Y. Ren, R.W. Shi, J.T. Yu, Z. Sun, S.Y. Guo, J.N. Guo, F. Yan, ACS Appl. Mater. Interfaces 13 (2021) 16289–16299.
[5] S.F. Zhang, J. Luo, F.J. Zhang, X.N. He, Compos. Commun. 32 (2022), 101183.
[6] J.Y. Zhao, D.J. Chen, B. Boateng, G.F. Zeng, Y.P. Han, C. Zhen, J.B. Goodenough, W. D He, J. Power Sources 451 (2020), 227773.
[7] G.H. Sun, S.J. Jiang, X.X. Feng, X.R. Shi, X. Zhang, T.T. Li, N.J. Chen, L.L. Hou, S. L. Qi, D.Z. Wu, J. Membr. Sci. 645 (2022), 120208.
[8] S.H. Lee, J. Kim, B.H. Kim, S. Yoon, K.Y. Cho, Small 15 (2019), 1804980.
[9] T.W. Zhang, J.L. Chen, T. Tian, B. Shen, Y.D. Peng, Y.H. Song, B. Jiang, L.L. Lu, H. B. Yao, S.H. Yu, Adv. Funct. Mater. 29 (2019), 1902023.
[10] J.Z. Sheng, Q. Zhang, M.S. Liu, Z.Y. Han, C. Li, C.B. Sun, B. Chen, X.W. Zhong, L. Qiu, G.M. Zhou, Nano Lett. 21 (2021) 8447–8454.
[11] X.N. Feng, M.G. Ouyang, X. Liu, L.G. Lu, Y. Xia, X.M. He, Energy Storage Mater. 10 (2018) 246–267.
[12] Z.D. Hao, Y. Wu, Q. Zhao, J.D. Tang, Q.Q. Zhang, X.X. Ke, J.B. Liu, Y.H. Jin, H. Wang, Adv. Funct. Mater. 31 (2021) 2102938–2102946.
[13] C.Q. Zhu, J.X. Zhang, S.Y. Qiu, Y.B. Jia, L.X. Wang, H. Wang, Compos. Commun. 24 (2021), 100659.
[14] J.Y. Pai, C.T. Hsieh, C.H. Lee, J.A. Wang, H.Y. Ku, C.L. Huang, L.J. Hardwick, C. C. Hu, J. Power Sources 482 (2021), 229054.
[15] M. Waqas, S. Ali, C. Feng, D.J. Chen, J.C. Han, W.D. He, Small 15 (2019), e1901689.
[16] C.M. Costa, Y.H. Lee, J.H. Kim, S.Y. Lee, S. Lanceros-Méndez, Energy Storage Mater. 22 (2019) 346–375.
[17] L.C. Kong, Y. Li, W. Feng, Electrochem. Energy Rev. 4 (2021) 633–679.
[18] Y. Hou, Z.D. Huang, Z. Chen, X.L. Li, A. Chen, P. Li, Y.B. Wang, C.Y. Zhi, Nano Energy 97 (2022), 107204.
[19] S. Ryu, T. Sugimoto, J. Kim, K. Park, D. Im, Y.G. Lee, J.W. Choi, ACS Appl. Energy Mater. 4 (2021) 5237–5245.
[20] J. Cho, Y.C. Jung, Y.S. Lee, D.W. Kim, J. Membr. Sci. 535 (2017) 151–157.
[21] S.S. Zhang, X.L. Fan, C.S. Wang, J. Mater. Chem. 6 (2018) 10755–10760.
[22] H. Lee, H. Jeon, S. Gong, M.H. Ryou, Y.M. Lee, Appl. Surf. Sci. 427 (2018) 139–146.
[23] M.M. Chi, L.Y. Shi, Z.Y. Wang, J.F. Zhu, X.F. Mao, Y. Zhao, M.H. Zhang, L.N. Sun, S. Yuan, Nano Energy 28 (2016) 1–11.
[24] H. Li, D.B. Wu, J. Wu, L.Y. Dong, Y.J. Zhu, X. Hu, Adv. Mater. 29 (2017), 1703548.
[25] M.N. Wang, X. Chen, H. Wang, H.B. Wu, X.Y. Jin, C. Huang, J. Mater. Chem. 5 (2017) 311–318.
[26] B. Zhang, Q.F. Wang, J.J. Zhang, G.L. Ding, G.J. Xu, Z.H. Liu, G.L. Cui, Nano Energy 10 (2014) 277–287.
[27] L.S. Kong, Y. Wang, H.S. Yu, B.X. Liu, S.L. Qi, D.Z. Wu, W.H. Zhong, G.F. Tian, J. Wang, ACS Appl. Mater. Interfaces 11 (2019) 2978–2988.
[28] Z.H. Lu, F. Sui, Y.E. Miao, G.H. Liu, C. Li, W. Dong, J. Cui, T.X. Liu, J.X. Wu, C. L. Yang, J. Energy Chem. 58 (2021) 170–197.
[29] M.N. Li, Z.J. Zhang, Y.T. Yin, W.C. Guo, Y.G. Bai, F. Zhang, B. Zhao, F. Shen, X. G. Han, ACS Appl. Mater. Interfaces 12 (2020) 3610–3616.
[30] J. Choi, K. Yang, H.S. Bae, I. Phiri, H.J. Ahn, J.C. Won, Y.M. Lee, Y.H. Kim, M. H. Ryou, Nanomaterials 10 (2020) 1976.
[31] Y. Maeyoshi, S. Miyamoto, H. Munakata, K. Kanamura, J. Power Sources 350 (2017) 103–108.
[32] Y.J. Li, H.T. Pu, J. Power Sources 384 (2018) 408–416.
[33] S.J. Rinehart, B.N. Nguyen, R.P. Viggiano, M.A.B. Meador, M.D. Dadmun, ACS Appl. Mater. Interfaces 12 (2020) 30457–30465.
[34] M. Palanisamy, K.W. Lin, C.T. Lo, V.G. Pol, ACS Appl. Mater. Interfaces 14 (2022) 28310–28320.
[35] Y.F. Li, Q.H. Li, Z.C. Tan, J. Power Sources 443 (2019), 227262.
[36] Y.E. Miao, G.N. Zhu, H.Q. Hou, Y.Y. Xia, T.X. Liu, J. Power Sources 226 (2013) 82–86.
[37] M.L. Li, L. Sheng, R. Xu, Y. Yang, Y.Z. Bai, S.J. Song, G.J. Liu, T. Wang, X.L. Huang, J.P. He, Compos. Commun. 24 (2021), 100607.
[38] C.Y. Tsai, Y.L. Liu, J. Membr. Sci. 640 (2021), 119816.
[39] L.K. Kong, Y.R. Yan, Z.M. Qiu, Z.Q. Zhou, J.Q. Hu, J. Membr. Sci. 549 (2018) 321–331.
[40] M.H. Parekh, S. Oka, J. Lutkenhaus, V.G. Pol, ACS Appl. Mater. Interfaces 14 (2022) 29176–29187.
[41] Y.J. Li, G. Zhang, B. Chen, W. Zhao, L.T. Sha, D. Wang, J. Yu, S.Q. Shi, Chin. Chem. Lett. 33 (2022) 3287–3290.
[42] B.T. Yuan, K.C. Wen, D.J. Chen, Y.P. Liu, Y.F. Dong, C. Feng, Y.P. Han, J.C. Han, Y. Q. Zhang, C. Xia, A. Sun, W.D. He, Adv. Funct. Mater. 31 (2021), 2101420.
[43] C.Y. Zhou, W. Zong, G.Y. Zhou, X.S. Fan, Y.-E. Miao, Compos. Commun. 25 (2021), 100696.
[44] L.D. Shen, X. Liu, J. Dong, Y.T. Zhang, C.X. Xu, C. Lai, S.Q. Zhang, J. Energy Chem. 52 (2021) 262–268.
[45] P. Chen, J.X. Shen, T.L. Wang, M. Dai, C.H. Si, J.X. Xie, M. Li, X.T. Cong, X. Sun, J. Power Sources 400 (2018) 325–332.
[46] P. Chen, H.M. Ren, L.T. Yan, J.X. Shen, T.L. Wang, G.D. Li, S.W. Chen, X.T. Cong, J. X. Xie, W. Li, ACS Sustainable Chem. Eng. 7 (2019) 16612–16619.
[47] P.L. Zhou, D.X. Yao, H.Q. Liang, J.W. Yin, Y.F. Xia, Y.P. Zeng, ACS Appl. Energy Mater. 5 (2022) 2011–2023.
[48] Q.C. Du, M.T. Yang, J.K. Yang, P. Zhang, J.Q. Qi, L. Bai, Z. Li, J.Y. Chen, R.Q. Liu, X.M. Feng, Z.D. Huang, T. Masese, Y.W. Ma, W. Huang, ACS Appl. Mater. Interfaces 11 (2019) 34895–34903.
[49] C.C. Li, B.S. Qin, Y.F. Zhang, A. Varzi, S. Passerini, J.Y. Wang, J.M. Dong, D. L. Zeng, Z.H. Liu, H.S. Cheng, Adv. Energy Mater. 9 (2019), 1803422.
[50] Y. Wang, S.Q. Wang, J.Q. Fang, L.X. Ding, H.H. Wang, J. Membr. Sci. 537 (2017) 248–254.
[51] C.H. Lee, Y.C. Huang, U. Kinzlinger, D. Esken, Y.H. Lin, A.T. Tsai, H.C. Wu, Y.C. Li, C.C. Hu, ACS Sustainable Chem. Eng. 9 (2021) 1590–1598.
[52] N.X. Wei, J.N. Hu, M.Z. Zhang, J.L. He, P.H. Ni, Electrochim. Acta 307 (2019) 495–502.